Synthesis, spectroscopic characterization, molecular docking, antioxidant and anticancer studies of some metal complexes from tetraazamacrocyclic Schiff base ligand

Omar S. Khalifa[1], Enass J. Waheed[2]
[1]Department of Chemistry, College of Science, University of Anbar, Anbar, Iraq.
[2]Department of Chemistry, College of Education for Pure Sciences, Ibn -Al-Haitham, University of Baghdad, Baghdad, Iraq.

Abstract

Five novel nickel, iron, cobalt, copper, and mercury complexes were synthesized from tetraazamacrocyclic Schiff base ligand (L), which were derived from 3-(4-(dimethyl amino) benzylidene) pentane-2,4-dione and 1,2-diaminocyclohexane in a 2:2 molar ratio. Many physico-chemical and spectroscopic techniques, including melting point, 1HNMR, 13CNMR, elemental analysis, molar conductance, magnetic susceptibility, UV-Vis, FT-IR, and thermogravimetric analysis (TGA), were used to characterize the Schiff base ligand and all metal complexes. The octahedral geometry of all the complexes [MLCl2] is confirmed by spectroscopic analyses. All substances' biological properties, such as their in vitro antioxidant activity or level of free radical scavenging, were assessed. Effect on standard ascorbic acid using the DPPH method and in vitro anticancer activities against colon cancer cell lines using the MTT assay. Furthermore, for the identification of binding modes of tetraazamacrocyclic Schiff base ligand L in the active pocket of target bacterial proteins such as beta-Lactamase and penicillin binding proteins, molecular docking studies were performed.

Key words: Tetraazamacrocyclic, Molecular Docking, Colon Cancer

Address for correspondence:

Omar S. Khalifa, Department of Chemistry, College of Science, University of Anbar, Anbar, Iraq; Email: omar.saeed@uoanbar.edu.iq

INTRODUCTION

When a cyclic molecule has nine or more atoms in its ring, three of those atoms must be electron pair donors; this is referred to as a macrocyclic compound [1]. Because they can selectively chelate particular metal ions depending on the quantity, kind, and position of their donors, the ionic radii of the metal centers, and the coordinating property of counterions, macrocyclic Schiff bases are crucial in macrocyclic chemistry [2-4]. However, fundamental research in fields like biology, catalysis, and magneto chemistry can greatly benefit from understanding the chemistry of transition metal complexes [5-8]. There are several significant macrocyclic metal complexes that exhibit intriguing biological properties, such as antibacterial, antifungal, anticancer, and antiproliferative actions [9-12]. In addition, synthetic tetraazamacrocycles (N4) have been regarded as generally reliable models because they have four nitrogen donor sites that are only allowed to stabilize unusual oxidation states of coordinated metal ions. Different physical and chemical methods, including FT-IR, UV-Vis, NMR, TgA, conductance measurements, and elemental analysis, were used to characterize all the complexes.

EXPERIMENTAL

Materials and methods

The chemicals, o-diamino cyclohexane (Sigma Aldrich), acetyl acetone (Thomas Baker), P-Dimethylamino benzaldehyde (CDH), were used as received. The metal salts $CoCl_2.6H_2O$ (Oxford), $NiCl_2$, $MnCl_2$, $HgCl_2$ and $CuCl_2 \cdot 2H_2O$ (CDH), $FeCl_2.4H2O$ (SigmaAldrich), were commercially available pure samples. Ethanol (Honey well) was used as solvent.

Physical measurements

The University of Baghdad's Micro-analytical Central Service Laboratory used a Perkin-Elmer 2400 CHN Elemental Analyzer to conduct the elemental studies. As KBr/CsI discs, the complexes' FTIR spectra (4000–200 cm1) were captured by a Perkin-Elmer Spectrum RX-I spectrophotometer. The Bruker Avance II 400 NMR spectrometer was used to record the 1H and 13C NMR spectra in DMSO-d6 using Me4Si as the internal standard, provided at Kharazmi University in Iran. On a Cary 5E UV-VIS-NIR spectrophotometer operating at room temperature, the electronic spectra of the complexes in DMSO were captured. At the Ibn Al-Haitham College of Education for Pure Science, University of Baghdad, the molar conductivities of the complexes (103M solutions in DMSO) were measured using a Philips pw-Digital Meter Conductivity.

Synthesis of precursor (P)

Acetyl acetone (1.1 gm, 11 mmol) and sodium hydroxide (1.6 gm, 41 mmol) were dissolved in the in 30 ml of ethanol were added into 100 ml one-necked flask equipped with condenser and magnetic bar. The mixture was heated for 10 min at 50°C.

Then, p-bromobenzaldehyde (2 gm, 11 mmol) was also added to the reaction flask. Overnight, the mixture was left at room temperature. A yellow precipitate was produced after the mixture was treated with an aqueous solution of HCl precipitate was washed with water until a neutral aqueous solution was obtained. Then, the product was filtered under vacuum, washed with cold water until the filtrate be neutral to litmus, finally recrystallized from ethanol [13].

Synthesis of tetraazamacrocyclic Schiff base ligand (L)

An equimolar amount of 1,2-diaminocyclohexane (4 g, 35 mmol) with 3-(4-bromobenzylidene) pentane-2,4-dione 1a (7.4 g, 35 mmol), both dissolved in absolute ethanol, was refluxed, heated in the presence of a catalytic amount of glacial acetic acid, stirred for 8 hours, allowed to cool to room temperature, the precipitate

washed with cold ethanol, allowed to dry, and finally recrystallized from ethanol [14, 15].

Synthesis of complexes

To an ethanolic solution (20 ml) of metal salts (8.6×10^{-1} mmol), the ethanolic solutions of 6,7,14,15-tetraphenyl-1,2,3,4,4a,8a,9, 10,11,12, 12a,16a-dodecahydrodibenzo [b,h] [1,4,7,10] tetraazacyclo dodecine L (5×10^{-1} g, 8.6×10^{-1} mmol) were added simultaneously with constant stirring. The reaction mixture was then refluxed for 4 hours. The mixture was let to cool at room temperature, and the precipitate was filtered, washed with hot ethanol, and dried in a vacuum [16, 17]. Table 1 displays some of the prepared complexes' physical characteristics, including the weight of metal salts and yield, (Figure 1) Where M^{II}= Co, Cu, Fe, Ni, and Hg.
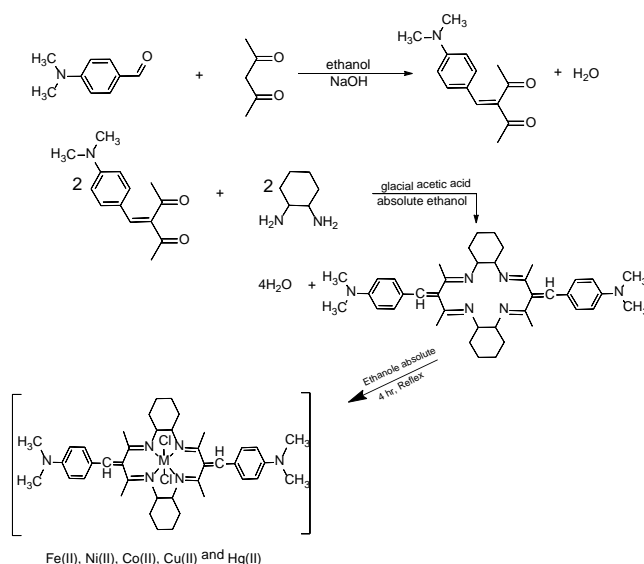

Fig. 1. Synthesis of ligand and its complex

RESULT AND DISCUSSION

Thermal stability and the nature of the colored solid are the most important characteristics of the prepared metal

complexes. In solvents (DMSO) and (DMF), soluble. The theoretical and practical data of (C.H.N) Microanalysis for all prepared complexes were approximated, (Table 1).

Tab. 1. Different physical properties of (L) and its complexes

Empirical formula	M.wt g/mol.	yield	color	m.p.	Microanalysis found, (Calc.) %		
		%		°C	C	H	N
$C_{40}H_{54}N_6Cl_2$	618.91	61.2	Dark orange	153	77.63	8.79	13.58
$[HgC_{40}H_{54}N_6Cl_2]$	890.4	72.3	Dark orange	288	54.08	6.23	9.56
					-53.96	-6.11	-9.44
$[CoC_{40}H_{54}N_6Cl_2]$	748.75	67.8	Black	265-267	64.23 (64.17)	7.35 (7.27)	11.29 (11.22)
$[CuC_{40}H_{54}N_6Cl_2]$	753.36	70.2	green	292-294	63.81	7.34	11.26
					-63.77	-7.23	-11.16
$[NiC_{40}H_{54}N_6Cl_2]$	748.51	68.8	Brown	192	64.27 (64.19)	7.34 (7.27)	11.45 (11.23)
	745.66	52.6	Light yellow	210	64.61	7.42	11.35

[FeC$_{40}$H$_{54}$N$_6$Cl$_2$]					-64.43	-7.3	-11.27

IR spectrum of precursor (p)

The aromatic ring generates an absorption band in the region of 3024 cm-1 due to the C-H stretching vibrations [18]. Major bands were observed in the range of 2977–2937 cm−1 and 2898 cm−1 which indicate the presence of aliphatic C-H groups [19]. The peak at the frequency of 1635 cm-1 attributable to the carbonyl group [20]. Also, a strong band for the C=C group of the chalcone compound appears at 1573 cm-1 [21]. The peaks at the frequencies 1523–1477 cm-1 and 1431 cm-1 are attributable to C=C groups for the phenyl rings [22], (Figure 2).
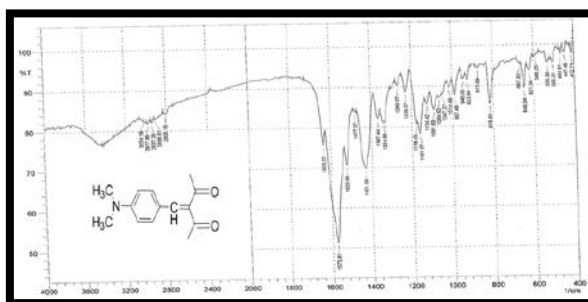

Fig. 2. FTIR spectrum of precursor (p)

IR spectrum of macrocyclic ligand (L)

The ligand's IR spectra (Table 2) reveal a strong intensity absorption band at 1575 cm1, which is attributed to the C=N stretching mode [23-29]. Aromatic rings have been identified by their characteristic ring vibrations in the 1488 and 1442–1427 cm−1 regions [30]. The absence of bands characteristic of (C=O) and amine bands (NH2) expected to appear in free chalcone compounds and o-cyclohexanediamine, respectively, confirms the formation of the proposed macrocyclic framework, (Figure 3).
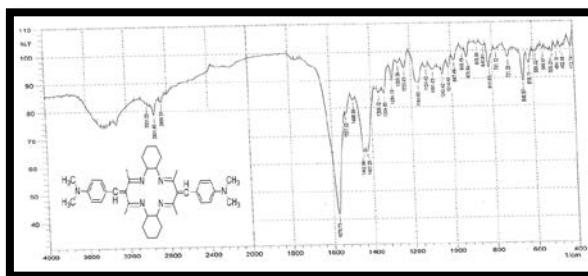
Fig. 3. FTIR spectrum of precursor (L)

IR spectrum of macrocyclic complexes

At 1606–1566 cm−1, an azomethine group C=N band was visible in the complexes [31-33]. The emergence of a new band of medium intensity in the range of 480–420 cm-1 as a result of vM−N vibration provides more evidence for nitrogen's coordination with the metal [34-36]. Furthermore, the presence of v (M-C1) results in a new band of medium intensity at 312-221 cm-1 [37-39], (Figure 4), (Table 2).

Fig. 4. FTIR spectrum of [FeLCl2] complex

Tab. 2. FT-IR data of (L) (cm-1) and its complexes
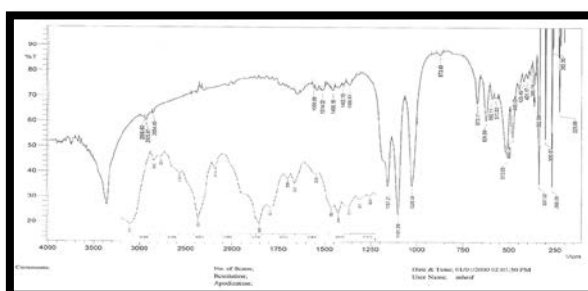
| Empirical formula	υ(C-H) alipha	(υC=N(	(C-C)υ	υ (M-N)	υ(M-Cl)
$C_{40}H_{54}N_6Cl_2$	,2901 2858	1575	,1442 1427	_	_
$[HgC_{40}H_{54}N_6Cl_2]$	,2929 2856	1596	,1483 1445	466	264
$[CoC_{40}H_{54}N_6Cl_2]$	,2941 2884	1583	,1454 1402	437	266
$[CuC_{40}H_{54}N_6Cl_2]$	,2929 2854	1577	,1444 1396	459	273
$[NiC_{40}H_{54}N_6Cl_2]$	,2931 2880	1602	,1452 1402	482	268
$[FeC_{40}H_{54}N_6Cl_2]$	,2958 2825	1558	,1456 1402	480	268

1H and 13C NMR spectra

The 1H-NMR spectra of compound L are listed in the experimental section. Resonances of the aromatic protons (H7 and H18) were observed within the chemical shift range δ = 7.64–6.74 ppm [40-42]. It is showing similar multiple signals corresponding to the (H10, H15, H26, and H31) proton of the cyclohexane at δ = 3.47–3.42 ppm [43]. The singlet signal at δ = 3.00–2.96 ppm was attributed to the methyl group protons (CH3). The signals at δ = 1.83–1.69 ppm were ascribed to the cyclohexane protons (H11, H14, H27, and H30). The 1H-NMR spectra also show that the cyclohexane protons (CH2) were observed as a signal at the chemical shift δ = 1.08–1.04 ppm [44, 45], (Figure 5).
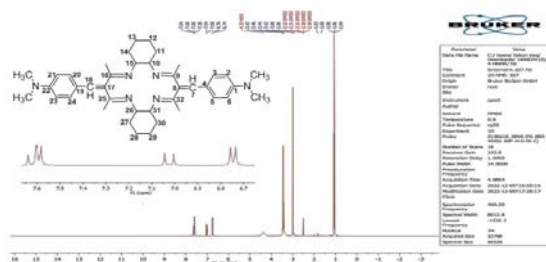
Fig. 5. ¹H-NMR spectrum of compound L at (400MHZ)

The ¹³C-NMR spectral data for each compound L₄ is listed in the experimental section, and the ¹³C-NMR spectra of compound L₄ are shown in Figures 6.6 and 6.7. The imine group (C=N) was observed at the chemical shift δ =163.07 ppm [46]. The signals were observed within δ =152.14-112.30 ppm were assigned to aromatic carbons in the phenyl ring and cyclo hexane carbons (C7, C8, C17 and C18) [47]. The peaks in the range of δ =56.49 ppm were assigned to C10, C15, C26, and C31 carbons in the cyclohexane [48]. In the ¹³C-NMR spectra, the peaks in the range of δ =44.89 ppm were attributed to the methyl group carbons (N-CH3). Similarly, the ¹³C-NMR signal for methylene group carbon CH2 (C11, C14, C27, and C30) was found at δ =31.86 ppm. The signals were observed at δ =23.69 ppm, which corresponds to C12, C13, C28, and C29, while the methyl group (CH3) appears in the region of δ =19.02 ppm [49], (Figure 6).
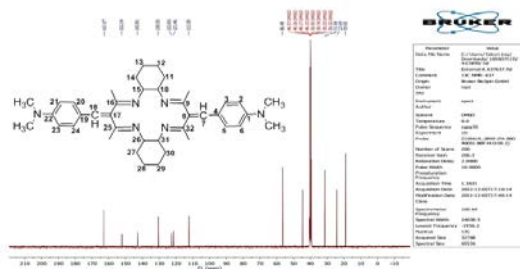
Fig. 6. ¹³C-NMR spectrum of compound L at (400MHZ)

ELECTRONIC SPECTRA

Ligand (L)

The electronic spectrum of ligand (L4) Figure (3.56) showed two intense peaks at (270nm = 37037 cm-1; εmax =500 molar-1.cm-1) and (298nm=33557 cm-1; εmax =730 molar^{-1} . cm^{-1}) are assigned to $\pi - \pi^*$ and $n - \pi^*$ transitions [140,154], In (Table 4), (Figure 7) data are recorded.
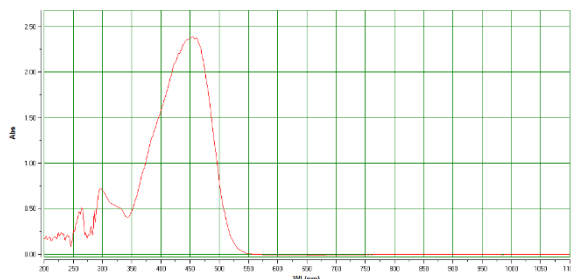

Fig.7. Electronic spectrum of L

Ligand (L) Complexes

The electronic spectrum of Fe^{II}-complex, exhibits four peaks, Figure (7). The firstly at (315 nm=31746 cm^{-1}; εmax =1380 molar^{-1}.cm^{-1}) was assigned to charge transfer transition. The peak is at visible at (770 nm=12987 cm^{-1}; εmax =180 molar^{-1}.cm^{-1}) assigned to the d-d electronic transition type $^5T_2g \rightarrow {}^5Eg$ transition, confirming an octahedral structure around Fe^{II} central metal ion [50, 51].

The electronic spectrum of Co^{II}-complex, exhibits four peaks. The firstly at (263 nm=38022 cm^{-1}; εmax =240 molar^{-1}.cm^{-1} is assigned to the ligand field. The peaks are at visible at (320 nm=31250 cm^{-1}; εmax =1600 molar^{-1}.cm^{-1}) , (450 nm=22222 cm^{-1}; εmax =800 molar^{-1}.cm^{-1}) and (680 nm=14705 cm^{-1}; εmax =320 molar^{-1}.cm^{-1}) assigned to the d-d electronic transition types C.T mix $^4T_1g_{(F)} \rightarrow {}^4T_1g_{(P)}$,$^4T_1g_{(F)} \rightarrow {}^4A_2g$ and $^4T_1g_{(F)} \rightarrow {}^4T_2g_{(F)}$ transition respectively, confirming an octahedral structure around Co^{II} central metal ion [50, 52].

The electronic spectrum of Ni^{II}-complex, exhibits five peaks. The firstly at (260 nm=38461 cm^{-1}; εmax =270 molar^{-1}.cm^{-1} and (330 nm=30303 cm^{-1}; εmax =850 molar^{-1}.cm^{-1}) are assigned to the ligand field and charge transfer transitions. The peaks are at visible at (450 nm=22222 cm^{-1}; εmax =830 molar^{-1}.cm^{-1}) , (660 nm=15151 cm^{-1}; εmax =160 molar^{-1}.cm^{-1}) and (935 nm=10695 cm^{-1}; εmax =120 molar^{-1}.cm^{-1}) assigned to the d-d electronic transition types C.T mix $^3A_2g \rightarrow {}^3T_1g_{(P)}$, $^3A_2g \rightarrow {}^3T_1g_{(F)}$ and $^3A_2g \rightarrow {}^3T_2g_{(F)}$ transition respectively, confirming an octahedral structure around Ni^{II} central metal ion [50, 53]. The electronic spectrum of Cu-complex showed three intense peaks in the range (260nm=38461 cm^{-1}; εmax =220 molar^{-1}.cm^{-1}) and (315nm=31746 cm^{-1}; εmax =2300 molar^{-1}. cm^{-1}) are assigned to the ligand field and charge transfer transitions. The peak is at visible region at (712nm=14044 cm^{-1}; εmax =210 molar^{-1}. cm^{-1}). This peak is assigned to the d-d electronic transition type ($^2Eg \rightarrow {}^2T_2g$) transition confirming an octahedral structure around Cu^{II} ion complex [50, 54].

The electronic spectrum of Hg^{II} - complex. In the spectrum showed three peaks at (268 nm=37313 cm^{-1}; εmax=800 molar^{-1}.cm^{-1}) , (278nm=35971 cm^{-1}; εmax=980 molar^{-1}.cm^{-1}) and (335nm=29850 cm^{-1}; εmax=2300 molar^{-1}.cm^{-1}) for Hg^{II}- complex, assigned to the ligand field ,charge transfer and charge transfer transitions. Finally, the metal ion of these complex belongs to d^{10} system does not show d–d transition, because full d orbitals, (Table 3) [50, 55].
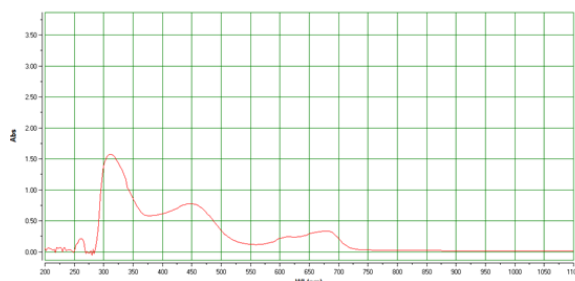

Fig. 8. Electronic spectrum of [CoLCl4] complex

Tab. 3. UV-Vis data of L and its complexes.

Com.	Wave number		A	$\varepsilon_{\mu\alpha\xi}$	Transitions	μ_{eff}	Conducts
	nm	cm^{-1}		molar^{-1} cm^{-1}		B.M.	Ohm^{-1}cm^{2}mol^{-1}
[C$_{40}$H$_{54}$N$_6$] L	270	37037	0.5	500	π —		------------
	298	33557	0.73	730	π*		
	450	22222	2.34	2340	n —		
					π*		
					n —		
					π*		
[FeC$_{40}$H$_{54}$N$_6$Cl$_2$]	315	31746	1.38	1380	C.T	5.17	15.6
	770	12987	0.18	180	$^5T_2g \rightarrow\ ^5Eg$		
[CoC$_{40}$H$_{54}$N$_6$Cl$_2$]	263	38022	0.24	240	L.F	4.85	13.4
	320	31250	1.6	1600	C.T mix $^4T_1g_{(F)} \rightarrow\ ^4T_1g_{(P)}$		
	450	22222	0.8	800	$^4T_1g_{(F)} \rightarrow\ ^4A_2g$		
	680	14705	0.32	320	$^4T_1g_{(F)} \rightarrow\ ^4T_2g_{(F)}$		
[NiC$_{40}$H$_{54}$N$_6$Cl$_2$]	260	38461	0.27	270	L.F	3.34	19.7
	330	30303	0.85	850	C.T		
	450	22222	0.83	830	C.T mix $^3A_2g \rightarrow\ ^3T_1g_{(P)}$		
	660	15151	0.16	160	$^3A_2g \rightarrow\ ^3T_1g_{(F)}$		
	935	10695	0.12	120	$^3A_2g \rightarrow\ ^3T_2g_{(F)}$		
[CuC$_{40}$H$_{54}$N$_6$Cl$_2$]	260	38461	0.22	220	L.F	1.79	21.1
	315	31746	2.3	2300	C.T		
	712	14044	0.21	210	$^2Eg \rightarrow\ ^2T_2g$		
[HgC$_{40}$H$_{54}$N$_6$Cl$_2$]	268	37313	0.8	800	L.F	0	7.8
	278	35971	0.98	980	C.T		
	335	29850	2.3	2300	C.T		

Magnetic moments and Conductivity measurements

In (Table 3), the values of measured magnetic susceptibility and the effective magnetic moment (μeff) for Fe (II), Co(II), Ni(II), and Cu(II) complexes are displayed. These complexes exhibit μeff (5.17, 4.85, 3.34 and 1.79) B.M respectively of L these normal values are consistent with octahedral complexes. The non-electrolytes nature of all metal complexes was confirmed by molecular conductivity measurements [56, 57].

Thermogravimetric

The Ni-complex was prepared subjected to thermal analysis using a STAPT-1000 Linseis company1 Germany [58]. In an atmosphere of argon gas, this measurement was done within temperature range 0°C -1000°C and heating rate 10°C/min. Where it was recorded all results are derived from the TG curves for these compounds examined in (Table 4), (Figure 9)

Tab. 4. Temperature values for analysis along with corresponding weight loss values

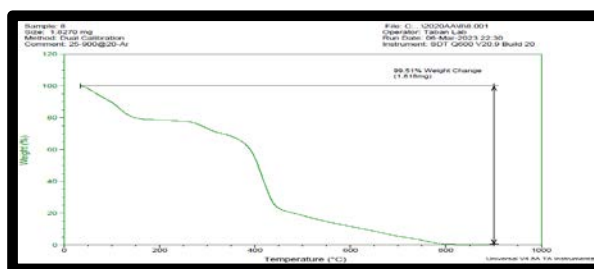| Compounds	Stage	TGA		
		TG range(°C)	% Estimated mass loss (mg) (calculated)	Fragmentation
			Mass loss	
C$_{40}$H$_{54}$Cl$_2$NiN$_6$	1	50-90	1.818 (1.818)	- 27H$_2$, Cl$_2$, 3N$_2$, Ni

Fig. 8. Thermal study of (L)

Molecular docking

In structural biochemistry and computer-aided drug design, molecular docking is a crucial computational method. The outcomes of our research were validated through molecular modeling studies. Hydrogen bonds and hydrophobic nonpolar interactions between the aromatic carbons of the macrocyclic ligands and the amino acids of the active protein were detected in the docking compounds.

In this study, we used CB-Dock, a novel blind docking technique that aims to improve docking precision [59]. With the aid of the cutting-edge docking program Autodock Vina, the online software CB-Dock Web has shown a successful action to predict the binding areas of a particular protein and determine the centers and sizes using a curvature-based cavity detection approach. A 3D representation of the binding possibilities is thus interactive, and CB-Dock also ranks the binding modes based on Vina ratings. The CB-Dock server can be accessed for free at http://cao.labshare.cn/cb-dock/.

The majority of the proteins have been uploaded into the PDB Database (www.RCSB.org), which is referred to as the protein data bank. The Protein Data Bank (PDB) [60] is continuously growing, and recent advances in structure prediction and experimental methods such as Cryo-EM will further accelerate this growth. Since ligands are present in the great majority of protein structures in the PDB, it is crucial to comprehend how these ligands work with their respective targets.

The chemicals, labeled as ligands in docking, are either obtained from the PupChem database at www.PubChem.org or can be generated by Chem. Draw Software. The PLIP website, the protein-ligand interaction profiler, is an efficient visualizer tool that can display the type of bonds, the distance between the atoms in the ligand and the protein, and the sites of atoms for both after docking has been completed by one of the aforementioned programs or websites. In addition, PLIP can identify halogen bonds, metal complexes, salt bridges, hydrophobic contacts, stacking, cation interactions, and hydrogen bonds. PLIP is easy to use as it requires only a PDB ID or a PDB file as input for the docked molecules, which comes from one of the docking softwares; it has been running reliably

and continuously for 5 years by a professional group; and it is transparent with all the source code published on GitHub. PLIP 2021 constitutes a main update with added support for nucleic acids, more flexibility through adjustable thresholds, mode and model selection, and a more functional and modern design for increased usability [61].

In-depth research on existing structures and the analysis and visualization of docking results are thus the two main cases for PLIP. However, PyMOl software, which is provided for free by the PyMOl Web for educational purposes, can be used to produce superior graphics. In this study, a docking investigation was performed to examine the effective residues that can bind the synthesized organic chemical compound in the active sites of the bacterial proteins such as beta-Lactamase, penicillin binding protein 2B (chain A) with PDB 1WAE, and Penicillin binding protein 2x (chain B) with PDB 1PYY enzymes that are found in the cell wall and try to understand their ability to inhibit the enzyme and consequently stop the growth. Moreover, it visualizes the three-dimensional conformation of the synthesized compound inside the active site of the lactamase, the type of the bonds, the length of the bonds, the distance in between, and also the free Gibbs energy values ΔG, which represent the stability of the binding. It is worth mentioning that the lower the energy values, the better the stability shown. The results of the docking study showed Gibbs free energy ΔG was for ligand L with the Penicillin binding protein 2B (chain A) with PDB 2WAE was -8.3 kcal/mol. The PLIP web results showed that compound L binds to the protein via hydrophobic bonds. However, no hydrogen bonds were shown for this ligand. This means that binding affinity is relatively weak.

The docking between the proteins and ligands showed hydrophobic interactions, which were visualized in Figure 10, and out of these ligands, L shows a good binding affinity. The L ligand was docked with the active site of the penicillin-binding protein 2B (chain A), PBP2, and showed hydrophobic interactions. The hydrophobic interactions were observed in LEU657A, ASN630A, PHE517A, ILE421A, and TYR422A with a bond length of 3.98A°, 3.71A°, 3.47A°, 3.68A° and 3.45A°, respectively, as seen in Table 5. The best distance between the ligand L4 and the amino acid in the bacterial proteins is 3.45 (Figure 11), (Table 5).

Tab. 5. Shows the details of the docking Ligand MacL4 with 2wae PDB using online software.

Index	Residue	AA	Distance	Ligand Atom	Protein Atom
1	421A	ILE	3.75	4638	2727
2	421A	ILE	3.68	4641	2728
3	422A	TYR	3.45	4625	2734
4	517A	PHE	3.47	4641	3466
5	630A	ASN	3.71	4649	4226
6	657A	LEU	3.98	4647	4430
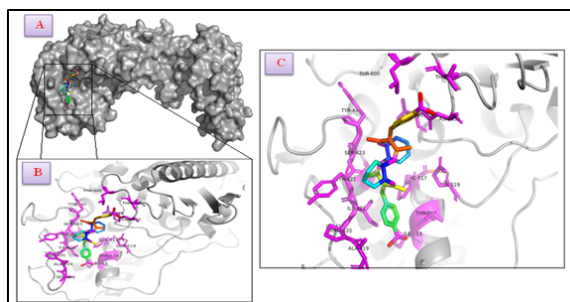
Fig. 9. Molecular simulations of the CB-docking of the ligand L with the penicillin-binding protein 2B (chain A) 2WAE PDB using PyMol software. A. shows the protein's binding pocket for the ligand L. B. displays a zoomed-in segment of a few contacts. C. shows the labeled residues and the ligand's interactions with the bacterial protein.
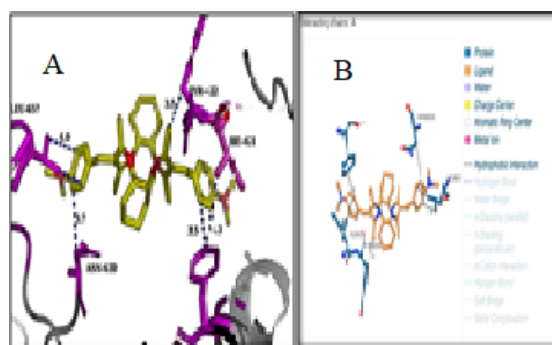
Fig. 11. A. cartoon representation of the docking analysis displayed using PyMol software. Only hydrophobic interactions were observed and are labelled with red dashed color. A bond length distances are shown near to the bonds and measured by angstrom. B. PLIP results. Representation of interaction between ligand L with the penicillin- binding protein 2B (chain A) 2WAE

Another bacterial protein was also docked by the synthesized compound L to investigate the affinity binding to inhibit the bacterial protein type Penicillin binding protein 2x (chain B) with PDB 1PYY. The results of this study showed better binding due to the observation of hydrogen bonds in the docking, as can be clearly seen in figure 4, in addition to the hydrophobic interaction. Hydrogen bonds can be formed between a hydrogen atom bound to an electronegative atom (such as oxygen, nitrogen, or fluorine) and another electronegative atom. Hydrogen bonds are usually present between the ligand molecule and specific amino acid residues in the protein's binding site.

The docking between the proteins and ligands showed hydrophobic interactions, which were visualized in Figure 12, and out of these ligands, L shows a good binding affinity. The L ligand was docked with the active site of the Penicillin binding protein 2x (chain B) with PDB 1PYY and showed a suitable binding affinity, including hydrophobic interactions, as analyzed in Figure 12. The hydrophobic interactions were shown in VAL376A, VAL476A, ASN377A, PHE570A, and TYR595A with a bond length of 3.45A°, 3.65A°, 3.23A°, 3.61A°, and 3.42A°, respectively, as seen in table 1.4. The best distance between the ligand L4 and the amino acid in the bacterial proteins is 3.23. Importantly, a hydrogen bond was observed in this interaction, as shown in Figure 12. Free Gibbs energy for ligands L, which were docked to Penicillin binding protein 2x (chain B) with PDB 1PYY, gave the values of -8.0 kcal/mol, (Figure12), (Table 6).

Tab. 6. shows the details of the docking Ligand MacL4 with IPYY PDB using online software.
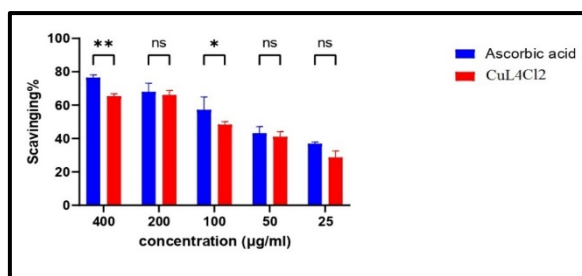
Hydrophobic interactions					
Index	Residue	AA	Distance	Ligand Atom	Protein Atom
1	376A	VAL	3.45	4656	1790
2	476A	VAL	3.65	4674	1791
3	377A	ASN	3.23	4665	1797
4	570A	PHE	3.61	4673	3259
5	595A	TYR	3.42	4661	3453
Hydrogen bonds					
Index	Residue	AA	Distance H-A	Distance D-A	Donor Angle	Ligand Atom	Protein Atom
1	597A	GLY	3.21	4.09	149.91	3464 [Nam]	4647 [N2]

Fig. 12. A. cartoon representation of the docking analysis displayed using PyMol software. Hydrophobic interactions and hydrogen bonds were observed and are labelled with red and green dashed color, respectively. A bond length distances are shown near to the bonds and measured by angstrom. B. PLIP results. Representation of interaction between ligand L4 with the penicillin-binding protein 2x (chain B) PDB 1PYY.

Measurements of antioxidant efficacy

Since the recently synthesized Schiff base macrocyclic complexes showed strong DNA-binding affinity, they are expected to possess antioxidant properties. By using the DPPH method at various doses, schiff-base macrocyclic complexes were further examined for their in vitro antioxidant activity and free-radical scavenging capabilities. According to Figure 2, the outcome varies directly with the various concentrations. All the analysis were performed, and they were averaged. In comparison to the reference (Ascorbic acid), the results showed that the metal complex utilized in this investigation had good radical scavenger activity. The reference at 200 g/mL had an inhibition percentage of 68.01%, but the highest inhibition percentage observed in complex 3 was lower at 66.08%. The coordination environment and redox characteristics may be to blame for the differences in activity amongst complexes. The complicated redox characteristics are often caused by a variety of factors, including axial ligation, charge type, coordination number, chelate ring size, degree of unsaturation, and chelate ring substitution pattern. 75 It can be inferred from this that these metal complexes may help improving their availability for medicinal purposes, (Figure 12) (Table 7) [62, 63].

Tab. 7. Scavenging activity of CuLCl2 compound

Concentration µg mL^{-1}	Scavenging % (Mean±SD)	
	Ascorbic acid	CuLCl$_2$
400	76.62±1.51	65.47±1.37
200	68.01±5.16	66.08±2.61
100	57.25±7.69	48.34±1.79
50	43.94±3.35	41.16±2.95
25	36.95±0.88	28.704±3.84

Fig. 13. The antioxidant activity of CuLCl2 complex compared with ascorbic acid as a reference

Cell viability and Cytotoxicity Assay (MTT)

By using the MTT assay, the copper complex's in vitro cytotoxic activity was examined against the colon cancer cell line, which is a human colon cancer cell line. The concentrations studied ranged from 400 g/ml to 12.5 g/ml.

The copper complex was examined on the colon cancer cell line and compared to the regular cell line for 24 hours at 37 °C. The toxicological effect of the selected complexes was estimated by extracting the percentage of growth inhibition rate compared to the control (100% growth) [64, 65].

Effect of CuLCl2 complex on growth of colon cancer cell line as well as normal cell line: The Table 8 shows the effect of the CuLCl2 complex on the growth of colon cancer cell lines and normal cell lines, as it was found that the lowest inhibition of cell growth was at the concentration (12.5 μg/ml) and the highest rate of inhibition was at the concentration (400μg/ml) for the cell lines tumor for colon and also normal cells. As evidence for this, normal cells were used to compare with cancer cells in the colon and to show the extent of the possibility of using it as a medicine. The inhibition ratios of the CuLCl2 complex were found to vary depending on the cell line type. For the cells of the colon cancer line and the normal cell line, the number of live cells left after reaction with the copper complex varies from 41.89% to 103%, while for the cells of the normal cell line, the number of live cells left after reaction with the copper complex varies from 25.83% to 54.28%, and it was found that the highest rate of inhibition of the cancer cell line and the normal cell line of the colon was at a concentration of 400 μg/ml. The percentages of cancer cells and normal cells at the same concentration as those above were 42.89% and 25.83%, respectively, after the copper complex reaction. Table 8 show the effect of the copper complex (ll) on the growth of colon cancer cell lines as well as normal cells (Figure 14).

Tab. 8. Effect of CuLCl2 complex on ovarian cancer cells line and compared to regular cells line for the same concentration using MTT test for 24 hrs at 37°C.

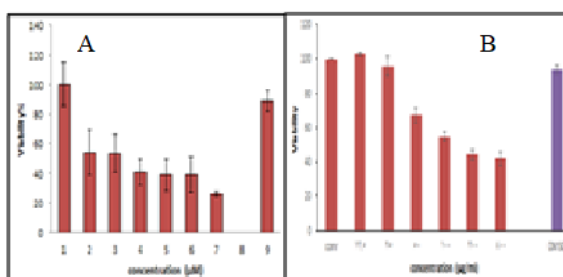| Concentration of Invented Macrocyclic complex	Normal cell		Colon cancer cell	
CuLCl$_2$ in (μg/Ml^{-1})	IC50= 126.21 μM		IC50= 59.2 μM	
	mean	SD	mean	SD
400	42.58	2.89	42.89	7.35
200	65.2	20.13	44.29	5.17
100	65.87	18.037	55.09	3.99
50	65.37	14.11	67.18	6.78
25	72.08	21.38	95.8	9.35
12.5	85.99	25.89	103	1.49

Fig. 14. A. Effect of CuLCl2 complex on to normal cells line for the same concentration using MTT test for 24 hrs at 37°C. B. Effect of CuLCl2 complex on colon cancer cells line for the same concentration using MTT test for 24 hrs. at 37°C.

CONCLUSION

In the present study, synthesis and characterization of five complexes of ligand (L) obtained by reaction 3-(4-(dimethyl amino) benzylidene) pentane-2,4-dione and 1,2-diaminocyclohexane using transition metal ions such as Fe(II), Ni(II), Co(II), Cu(II) and Hg(II) . The ligand (L) being tetra dentate and potent donors were found be (C=N) groups. The biological activities of all compounds were evaluated, like in-vitro antioxidant activity or percentage free radical scavenging. Effect via the DPPH method against standard ascorbic acid and in vitro anticancer activity via the MTT assay against colon cancer cell lines. Furthermore, for the identification of binding modes of tetraazamacrocyclic Schiff base ligand L in the active pocket of target bacterial proteins such as beta-Lactamase and penicillin binding proteins, molecular docking studies were performed.

ACKNOWLEDGEMENT

REFERENCES

1. Vögtle, F., & Weber, E. (Eds.). (2012). Host Guest Complex Chemistry Macrocycles: Synthesis, Structures, and Applications. Springer Science & Business Media.

2. Rosu, T., Pahontu, E., Ilies, D. C., Georgescu, R., Mocanu, M., Leabu, M, Gulea, A. (2012). Synthesis and characterization of some new complexes of Cu (II), Ni (II) and V (IV) with Schiff base derived from indole-3-carboxaldehyde. Biological activity on prokaryotes and eukaryotes. European journal of medicinal chemistry, 53, 380-389.

3. Firdaus, F., Fatma, K., Azam, M., Khan, S. N., Khan, A. U., & Shakir, M. (2008). Template synthesis and physicochemical studies of 14-membered hexaazmacrocyclic complexes with Co (II), Ni (II), Cu (II) and Zn (II): a comparative spectroscopic approach on DNA binding with Cu (II) and Ni (II) complexes. Transition Metal Chemistry, 33, 467-473.

4. Shakir, M., Khanam, S., Azam, M., Aatif, M., & Firdaus, F. (2011). Template synthesis and spectroscopic characterization of 16-membered [N4] Schiff-base macrocyclic complexes of Co (II), Ni (II), Cu (II), and Zn (II): in vitro DNA-binding studies. Journal of Coordination Chemistry, 64(18), 3158-3168.

5. Abdel-Rahman, L. H., Abu-Dief, A. M., Adam, M. S. S., & Hamdan, S. K. (2016). Some new nano-sized mononuclear Cu (II) Schiff base complexes: design, characterization, molecular modeling and catalytic potentials in benzyl alcohol oxidation. Catalysis Letters, 146, 1373-1396.

6. Ibrahim, E. M. M., Rahman, L. A., & Abu, A. M. (2018). Dief, RM El-Khatib, SM Abdel-Fatah, AM Adam. Appl. Organometal. Chem, 32, e4171.

7. Rahman, L. H. A., Abu-Dief, A. M., El-Khatib, R. M., & Abdel-Fatah, S. M. (2018). Sonochemical Synthesis, Spectroscopic Characterization, 3D Molecular Modeling, DNA Binding and Antimicrobial Evaluation of some Transition Metal Complexes Based on Bi-dentate NO Donor Imine Ligand. Int. J. Nano. Chem, 4(1), 1-17.

8. Elshafaie, A., Abdel-Rahman, L. H., Abu-Dief, A. M., Hamdan, S. K., Ahmed, A. M., & Ibrahim, E. M. M. (2018). Electric, thermoelectric and magnetic properties of Nickel (II) Imine Nanocomplexes. Nano, 13(07), 1850074.

9. Abou-Hussein, A. A., & Linert, W. (2015). Synthesis, spectroscopic studies and inhibitory activity against bactria and fungi of acyclic and macrocyclic transition metal complexes containing a triamine coumarine Schiff base ligand. Spectrochimica Acta Part A: Molecular and Biomolecular Spectroscopy, 141, 223-232.

10. Shreaz, S., Shiekh, R. A., Raja, V., Wani, W. A., & Behbehani, J. M. (2016). Impaired ergosterol biosynthesis mediated fungicidal activity of Co (II) complex with ligand derived from cinnamaldehyde. Chemico-biological interactions, 247, 64-74.

11. El-Boraey, H. A. (2012). Coordination behavior of tetraaza [N4] ligand towards Co (II), Ni (II), Cu (II), Cu (I) and Pd (II) complexes: Synthesis, spectroscopic characterization and anticancer activity. Spectrochimica Acta Part A: Molecular and Biomolecular Spectroscopy, 97, 255-262.

12. Andrew, F. P., & Ajibade, P. A. (2018). Synthesis, characterization and anticancer studies of bis-(N-methyl-1-phenyldithiocarbamato) Cu (II), Zn (II), and Pt (II) complexes: Single crystal X-ray structure of the copper complex. Journal of Coordination Chemistry, 71(16-18), 2776-2786.

13. Jamel, N. M., Hussein, D. F., & Tomma, J. H. (2017). Synthesis and Characterization New Schiff Bases, Pyrazole and Pyrazoline Compounds Derived From Acid Hydrazide Containing Isoxazoline Ring. Ibn AL-Haitham Journal For Pure and Applied Science, 27(3), 435-447.

14. Chaabane, L., Chahdoura, H., Moslah, W., Snoussi, M., Beyou, E., Lahcini, M., ... & Baouab, M. H. V. (2019). Synthesis and characterization of Ni (II), Cu (II), Fe (II) and Fe3O4 nanoparticle complexes with tetraaza macrocyclic Schiff base ligand for antimicrobial activity and cytotoxic activity against cancer and normal cells. Applied Organometallic Chemistry, 33(5), e4860.

15. Ben Haj Fraj, S., Chaabene, M., Agren, S., El Haskouri, J., Lahcini, M., Ben Chaâbane, R., & Baouab, M. H. V. (2022). High incorporation of magnetite nanoparticles inside tetraaza macrocyclic Schiff base cavity: spectroscopic characterization and modeling by DFT calculation. Journal of the Iranian Chemical Society, 1-20.

16. Palaniammal, A., & Vedanayaki, S. SYNTHESIS, SPECTRAL CHARACTERIZATION, BIOLOGICAL ACTIVITY OF MACROCYCLIC LIGANDS AND METAL COMPLEXES DERIVED FROM 3, 4-DIAMINOBENZOPHENONE AND DIKETONES.

17. Gull, P., Malik, M. A., Dar, O. A., & Hashmi, A. A. (2017). Design, synthesis and spectroscopic characterization of metal (II) complexes derived from a tetradentate macrocyclic ligand: Study on antimicrobial and antioxidant capacity of complexes. Microbial pathogenesis, 104, 212-216.

18. Alaşalvar, C., Öztürk, N., Alaa, A. M., Gökce, H., El-Azab, A. S., El-Gendy, M. A., & Sert, Y. (2018). Molecular structure, Hirshfeld surface analysis, spectroscopic (FT-IR, Laser-Raman, UV–vis. and NMR), HOMO-LUMO and NBO investigations on N-(12-amino-9, 10-dihydro-9, 10-ethanoanthracen-11-yl)-4-

methylbenzenesulfonamide. Journal of Molecular Structure, 1171, 696-705.

19. Straka, P., Buryan, P., & Bičáková, O. (2018). The formation of quasi-alicyclic rings in alkyl-aromatic compounds. Journal of Molecular Structure, 1154, 455-462.

20. ABD AL HUSSAIN, H. A. A., & ALJAMALI, D. N. M. (2021). Chalcone-heterocyclic derivatives (synthesis, spectral identification, microbial evaluation). International Journal of Pharmaceutical Research, 13(1).

21. Balaji, R., & Nanjundan, S. (2001). Synthesis and characterization of photocrosslinkable functional polymer having pendant chalcone moiety. Reactive and Functional Polymers, 49(1), 77-86.

22. Eren, B., Ünal, A., & Özdemir-Koçak, F. (2019). Combined experimental and theoretical studies on the chemical and spectroscopic properties of an antimicrobial N-(Phenyl) dimethyldisulfonimide. Journal of Molecular Structure, 1175, 542-550.

23. Shalabi, K., El-Gammal, O. A., & Abdallah, Y. M. (2021). Adsorption and inhibition effect of tetraaza-tetradentate macrocycle ligand and its Ni (II), Cu (II) complexes on the corrosion of Cu10Ni alloy in 3.5% NaCl solutions. Colloids and Surfaces A: Physicochemical and Engineering Aspects, 609, 125653.

24. Zafar, H., Kareem, A., Sherwani, A., Mohammad, O., Ansari, M. A., Khan, H. M., & Khan, T. A. (2015). Synthesis and characterization of Schiff base octaazamacrocyclic complexes and their biological studies. Journal of Photochemistry and Photobiology B: Biology, 142, 8-19.

25. Chandra, S., Gautam, A., & Tyagi, M. (2009). Synthesis, structural characterization, and antibacterial studies of a tetradentate macrocyclic ligand and its Co (II), Ni (II), and Cu (II) complexes. Russian Journal of Coordination Chemistry, 35, 25-29.

26. Chandra, S., Kumar, R., Singh, R., & Jain, A. K. (2006). Coordination stability between metal/ligands interaction by modern spectroscopic studies: IR, electronic, EPR and cyclic voltammetry of cobalt (II) complexes with organic skeleton containing cyclic ligands. Spectrochimica Acta Part A: Molecular and Biomolecular Spectroscopy, 65(3-4), 852-858.

27. Singh, D. P., Malik, V., Kumar, K., Sharma, C., & Aneja, K. R. (2010). Macrocyclic metal complexes derived from 2, 6-diaminopyridine and isatin with their antibacterial and spectroscopic studies. Spectrochimica Acta Part A: Molecular and Biomolecular Spectroscopy, 76(1), 45-49.

28. Menezes, A. P., Jayarama, A., & Ravindra, H. J. (2021). Investigation of physical, spectral and thermal properties of a dimethoxy substituted chalcone for opto-electronic device applications. Materials Today: Proceedings, 35, 374-377.

29. Tsukerman, S. V., Nikitchenko, V. M., Rozum, Y. S., & Lavrushin, V. F. (1967). Infrared spectra of thiophene analogs of chalcones and their vinylogs. Chemistry of Heterocyclic Compounds, 3(3), 361-366.

30. MIHSEN, H. H., ABASS, S. K., ABASS, A. K., HUSSAIN, K. A., & ABBAS, Z. F. (2018). Template Synthesis of Sn (II), Sn (IV) and Co (II) complexes via 3-Aminopropyltriethoxysilane and Salicylaldehyde and Evaluate their Antibacterial Sensitivity. Asian Journal of Chemistry, 30(10), 2277-2280.

31. Reddy, P. M., Shanker, K., Rohini, R., & Ravinder, V. (2009). Antibacterial active tetraaza macrocyclic complexes of Chromium

(III) with their spectroscopic approach. Int. J. Chem. Tech. Res, 1, 367-372.

32. Abdel-Rahman, L. H., Ismail, N. M., Ismael, M., Abu-Dief, A. M., & Ahmed, E. A. H. (2017). Synthesis, characterization, DFT calculations and biological studies of Mn (II), Fe (II), Co (II) and Cd (II) complexes based on a tetradentate ONNO donor Schiff base ligand. Journal of Molecular Structure, 1134, 851-862.

33. Gupta, A. K. Large Ring TetraazamacrocyclicComplexes of Cu (II) Derived From 2, 3-Pentanedione and Diaminoalkanes.

34. Singh, D., Kumar, K., Kumar, R., & Singh, J. (2010). Template synthesis and characterization of biologically active transition metal complexes comprising 14-membered tetraazamacrocyclic ligand. Journal of the Serbian Chemical Society, 75(2), 217-228.

35. Tyagi, M., & Chandra, S. (2014). Synthesis and spectroscopic studies of biologically active tetraazamacrocyclic complexes of Mn (II), Co (II), Ni (II), Pd (II) and Pt (II). Journal of Saudi Chemical Society, 18(1), 53-58.

36. Rana, V. B., Singh, P., Singh, D. P., & Teotia, M. P. (1982). Trivalent chromium, manganese, iron and cobalt chelates of a tetradentate N 6 macrocyclie ligand. Transition Metal Chemistry, 7, 174-177.

37. Gupta, S., Bansal, U., & Sarma, B. K. (2018). DESIGNING, SYNTHESIS AND SPECTROSCOPIC STUDIES OF Co (II), Ni (II) AND Cu (II) TRANSITION METAL COMPLEXES WITH NITROGEN DONOR TETRADENTATE, NOVEL MACROCYCLIC SCHIFF'S BASE LIGAND.

38. Sangwan, V., & Singh, D. P. (2019). In-vitro DNA binding and antimicrobial studies of trivalent transition metal ion based macrocyclic complexes. Vietnam Journal of Chemistry, 57(5), 543-551.

39. Aqra, F. M. (1999). New macrocyclic complexes containing amide, imine and secondary amine functions. Transition Metal Chemistry, 24(3), 337-339.

40. Ahmed, A. A., Mekky, A. E., Elwahy, A. H., & Sanad, S. M. (2020). Facile synthesis and characterization of novel benzo-fused macrocyclic dicarbonitriles and pyrazolo-fused macrocycles containing thiazole subunits. Synthetic Communications, 50(6), 796-804.

41. Keypour, H., Rezaeivala, M., Mirzaei-Monsef, M., Sayin, K., Dilek, N., & Unver, H. (2015). Synthesis and characterization of Co (II), Ni (II), Cu (II) and Zn (II) complexes with a new homopiperazine macrocyclic Schiff base ligand. Inorganica Chimica Acta, 432, 243-249.

42. N. Bandeira, P., LG Lemos, T., S. Santos, H., CS de Carvalho, M., P. Pinheiro, D., O. de Moraes Filho, M., ... & MR Teixeira, A. (2019). Synthesis, structural characterization, and cytotoxic evaluation of chalcone derivatives. Medicinal Chemistry Research, 28, 2037-2049.

43. Chaabane, L., Chahdoura, H., Moslah, W., Snoussi, M., Beyou, E., Lahcini, M., ... & Baouab, M. H. V. (2019). Synthesis and characterization of Ni (II), Cu (II), Fe (II) and Fe3O4 nanoparticle complexes with tetraaza macrocyclic Schiff base ligand for antimicrobial activity and cytotoxic activity against cancer and normal cells. Applied Organometallic Chemistry, 33(5), e4860.

44. Yerrasani, R., Karunakar, M., Dubey, R., Singh, A. K., Nandi, R., Singh, R. K., & Rao, T. R. (2016). Synthesis, characterization and photophysical studies of rare earth metal complexes with a mesogenic Schiff-base. Journal of Molecular Liquids, 216, 510-515.

45. Qiao, X., Sun, P., Wu, A., Sun, N., Dong, B., & Zheng, L. (2018).Supramolecular Thermotropic Ionic Liquid Crystals Formed via Self-Assembled Zwitterionic Ionic Liquids. Langmuir, 35(5), 1598-1605.

46. Manesh, A. A., & Zebarjadian, M. H. (2020). Synthesis of three new branched octadentate (N8) Schiff Base and competitive Lithium-7 NMR study of the stoichiometry and stability constant of Mn2+, Zn2+ and Cd2+ complexes in acetonitrile–[(BMIM)(PF6)] mixture. Journal of Molecular Structure, 1199, 126965.

47. BAOUAB, M. H. V., Fra, S. B. H., Chaabene, M., Agren, S., Lahcini, M., & Chaâbane, R. B. (2022). High incorporation of magnetite nanoparticles inside tetraaza macrocyclic Schiff base cavity: Spectroscopic characterization and modeling by DFT calculation.

48. Ramaiah, K., Srishailam, K., Reddy, K. L., Reddy, B. V., & Rao, G. R. (2019). Synthesis, crystal and molecular structure, and characterization of 2-((2-aminopyridin-3-yl) methylene)-N-ethylhydrazinecarbothioamide using spectroscopic (1H and 13C NMR, FT-IR, FT-Raman, UV–Vis) and DFT methods and evaluation of its anticancer activity. Journal of Molecular Structure, 1184, 405-417.

49. Velasquez-Silva, A., Forero, R. S., Sanabria, E., Perez-Redondo, A., & Maldonado, M. (2019). Host-guest inclusion systems of tetra (alkyl) resorcin [4] arenes with choline in DMSO: Dynamic NMR studies and X-ray structural characterization of the 1: 1 inclusion complex. Journal of Molecular Structure, 1198, 126846.

50. Lincoln, K. M., Offutt, M. E., Hayden, T. D., Saunders, R. E., & Green, K. N. (2014). Structural, spectral, and electrochemical properties of nickel (II), copper (II), and zinc (II) complexes containing 12-membered pyridine-and pyridol-based tetra-aza macrocycles. Inorganic Chemistry, 53(3), 1406-1416.

51. Sharma, V., Vashistha, V. K., & Das, D. K. (2020). Biological and electrochemical studies of macrocyclic complexes of iron and cobalt. Biointerface Res. App. Chem, 11, 7393-7399.

52. Vashistha, V. K., & Kumar, A. (2020). Synthesis of Co (II) and Ni (II) asymmetric tetraazamacrocyclic complexes and their electrochemical and antimicrobial studies. Russian Journal of Inorganic Chemistry, 65, 2028-2032.

53. Lincoln, K. M., Offutt, M. E., Hayden, T. D., Saunders, R. E., & Green, K. N. (2014). Structural, spectral, and electrochemical properties of nickel (II), copper (II), and zinc (II) complexes containing 12-membered pyridine-and pyridol-based tetra-aza macrocycles. Inorganic Chemistry, 53(3), 1406-1416.

54. Martinez-Camarena, A., Savastano, M., Blasco, S., Delgado-Pinar, E., Giorgi, C., Bianchi, A., ... & Bazzicalupi, C. (2021). Assembly of Polyiodide Networks with Cu (II) Complexes of Pyridinol-Based Tetraaza Macrocycles. Inorganic Chemistry, 61(1), 368-383.

55. Raman, N., Dhaveethu Raja, J., & Sakthivel, A. (2008). Template synthesis of novel 14-membered tetraazamacrocyclic transition metal complexes: DNA cleavage and antimicrobial studies. Journal of the Chilean Chemical Society, 53(3), 1568-1571.

56. El-Gammal, O. A., Al-Hossainy, A. F., & El-Brashy, S. A. (2018). Spectroscopic, DFT, optical band gap, powder X-ray diffraction and bleomycin-dependant DNA studies of Co (II), Ni (II) and Cu (II) complexes derived from macrocyclic Schiff base. Journal of Molecular Structure, 1165, 177-195.

57. Swamy, S. J., & Pola, S. (2008). Spectroscopic studies on Co (II), Ni (II), Cu (II) and Zn (II) complexes with a N4-macrocyclic ligands. Spectrochimica Acta Part A: Molecular and Biomolecular Spectroscopy, 70(4), 929-933.

58. Shakir, M., & Chingsubam, P. (2006). Metal ion-directed synthesis of 16-membered tetraazamacrocyclic complexes and their physico-chemical studies. Spectrochimica Acta Part A: Molecular and Biomolecular Spectroscopy, 64(2), 512-517.

59. Liu, Y., Grimm, M., Dai, W. T., Hou, M. C., Xiao, Z. X., & Cao, Y. (2020). CB-Dock: A web server for cavity detection-guided protein–ligand blind docking. Acta Pharmacologica Sinica, 41(1), 138-144.

60. Adasme, M. F., Linnemann, K. L., Bolz, S. N., Kaiser, F., Salentin, S., Haupt, V. J., & Schroeder, M. (2021). PLIP 2021: Expanding the scope of the protein–ligand interaction profiler to DNA and RNA. Nucleic acids research, 49(W1), W530-W534.

61. Young, J., Garikipati, N., & Durrant, J. D. (2022). BINANA 2: characterizing receptor/ligand interactions in Python and JavaScript. Journal of Chemical Information and Modeling, 62(4), 753-760.

62. Kothari, R., & Agrawal, A. (2020). Synthesis, molecular docking, antioxidant and anticanceractivitiesof tetraaza macrocyclic copper (Ii) complexes. Rasayan Journal of Chemistry, 13(3), 1672-1684.

63. Johnston, H. M., Pota, K., Barnett, M. M., Kinsinger, O., Braden, P., Schwartz, T. M., ... & Green, K. N. (2019). Enhancement of the antioxidant activity and neurotherapeutic features through pyridol addition to tetraazamacrocyclic molecules. Inorganic chemistry, 58(24), 16771-16784.

64. Remiya, J. P., Shyni, B., Sikha, T. S., & Parvathy, U. R. (2023). One-pot synthesis, characterization, photocatalytic activity and biological studies of Co (II), Ni (II) and Cu (II) complexes of a tetraazamacrocyclic Schiff base. Journal of Coordination Chemistry, 76(5-6), 729-748.

65. Chaabane, L., Chahdoura, H., Moslah, W., Snoussi, M., Beyou, E., Lahcini, M., ... & Baouab, M. H. V. (2019). Synthesis and characterization of Ni (II), Cu (II), Fe (II) and Fe3O4 nanoparticle complexes with tetraaza macrocyclic Schiff base ligand for antimicrobial activity and cytotoxic activity against cancer and normal cells. Applied Organometallic Chemistry, 33(5), e4860.